Quantitative non-contrast perfusion MRI in the body using arterial spin labeling

María Guadalupe Mora Álvarez[1] · Ananth J. Madhuranthakam[1,2] · Durga Udayakumar[1,2]

Abstract

Arterial spin labeling (ASL) is a non-invasive magnetic resonance imaging (MRI) method that enables the assessment and the quantification of perfusion without the need for an exogenous contrast agent. ASL was originally developed in the early 1990s to measure cerebral blood flow. The utility of ASL has since then broadened to encompass various organ systems, offering insights into physiological and pathological states. In this review article, we present a synopsis of ASL for quantitative non-contrast perfusion MRI, as a contribution to the special issue titled "Quantitative MRI—how to make it work in the body?" The article begins with an introduction to ASL principles, followed by different labeling strategies, such as pulsed, continuous, pseudo-continuous, and velocity-selective approaches, and their role in perfusion quantification. We proceed to address the technical challenges associated with ASL in the body and outline some of the innovative approaches devised to surmount these issues. Subsequently, we summarize potential clinical applications, challenges, and state-of-the-art ASL methods to quantify perfusion in some of the highly perfused organs in the thorax (lungs), abdomen (kidneys, liver, pancreas), and pelvis (placenta) of the human body. The article concludes by discussing future directions for successful translation of quantitative ASL in body imaging.

Keywords Perfusion · Arterial spin labeling · ASL · Quantitative · Non-contrast

Introduction

Perfusion plays a pivotal role in the delivery of oxygen and nutrients to the tissue and facilitates the removal of by products such as carbon dioxide. Quantifying perfusion is essential to understand various pathological conditions for effective clinical management. Diseases affecting organs in the body, such as liver, kidneys, lungs, and pancreas, often exhibit altered tissue perfusion, highlighting the importance of accurate quantitative perfusion measurement techniques. Magnetic resonance imaging (MRI) enables measurement of tissue perfusion and has predominantly relied on the injection of gadolinium-based contrast agents (GBCAs). Dynamic susceptibility contrast (DSC) or dynamic contrast enhanced (DCE) MRI acquired following the injection of GBCA can quantify perfusion [1, 2]; however, the reliability and the reproducibility of these quantitative measurements are highly variable [3, 4]. The administration of GBCAs also limits their routine use in specific patient groups, such as pediatrics, pregnant individuals, and those with impaired renal function. Notably, gadolinium (Gd) deposition has been observed in several tissues including skin, bone, and brain, particularly in patients receiving multiple GBCA injections during longitudinal imaging studies [5, 6]. Given that the long-term consequences of these Gd depositions are still unclear, there are some concerns with the repeated administration of GBCAs [7]. These challenges associated with contrast agent-based perfusion measurement have emphasized the need for alternative non-contrast quantitative perfusion imaging methods.

Arterial spin labeling (ASL) is a non-invasive proton MRI method that measures perfusion utilizing the water in the blood as an endogenous contrast agent. ASL involves magnetically labeling the arterial blood with radiofrequency (RF) saturation or inversion pulses. Two images are acquired in an ASL experiment: a label image, where the arterial blood is labeled using RF saturation or inversion, and a

✉ Durga Udayakumar
Durga.Udayakumar@UTSouthwestern.edu

1 Department of Radiology, UT Southwestern Medical Center, 5323 Harry Hines Blvd, Dallas, TX 75390-9061, USA

2 Advanced Imaging Research Center, UT Southwestern Medical Center, Dallas, TX, USA

control image, where the image is acquired without labeling the arterial blood. The difference between these two images generates a perfusion-weighted image, where the signal is directly proportional to the blood flow or perfusion. The time parameters of an ASL experiment can be optimized to minimize vascular signal contribution and thus accurately represent true perfusion signal. ASL has the advantage of providing absolute quantitative perfusion values in physiological units of milliliters per 100 g of tissue per minute (mL/100 g/min).

ASL was originally developed in the early 1990s to measure cerebral blood flow (CBF) in the brain [8–10]. Subsequently, ASL techniques and insights gained from the brain application were extended to measure perfusion in other organs, beginning with the kidneys [11], followed by applications in the placenta [12], liver [13], pancreas [14], and lungs [15]. Over the past three decades, great progress has enabled the adaptation of ASL to body applications [16, 17]; however, clinical applications of quantitative ASL in the body are still limited. There are several challenges that hinder the successful reproducibility of ASL in body applications. These include physiological motion, low signal-to-noise ratio (SNR), poor labeling efficiency, lack of standardized protocols, and diverse anatomy within the population. In this review article, we will provide an overview of different ASL labeling schemes, address current methodological challenges, and review state-of-the-art quantitative ASL-MRI in various highly perfused organs in the thorax, abdomen, and pelvis of the human body. The content of this article is aligned with the theme of this special issue, which is focused on "Quantitative MRI—how to make it work in the body?".

ASL methods

Labeling schemes

ASL is a subtraction-based imaging technique, wherein the perfusion signal within both the control and the labeled images comprises only a small fraction, typically ranging from 1 to 2% of the overall tissue signal. Consequently, this approach suffers from low SNR. This issue is further exacerbated by suboptimal labeling efficiency, increased off-resonance (B0) and RF transmit (B1 +) field inhomogeneities, and the presence of motion artifacts, which are particularly pronounced in body applications. To overcome these limitations, the design of ASL pulse sequences has led to various labeling schemes. The most commonly employed ASL labeling can be categorized into three groups: pulsed labeling (PASL) [18–21], continuous/pseudo-continuous labeling (CASL/pCASL) [8, 22], and

velocity-selective labeling (VS-ASL) [23]. Each of these methods has distinct advantages and may be suitable for specific applications.

Pulsed arterial spin labeling (PASL)

In pulsed ASL, an inversion pulse is used to label a slab (i.e., bolus) of arterial blood. There are several variations within the PASL labeling scheme; however, the most commonly used and a robust method for perfusion quantification is the flow-sensitive alternating inversion recovery (FAIR) [20]. FAIR uses a non-selective inversion pulse for the label image and a selective inversion pulse applied in the imaging slab for the control image. After an inversion time (TI), the labeled blood from outside the imaging plane enters and perfuses into the tissue being imaged. During this TI, saturation pulses are applied after certain time TI1, to define temporal width of the labeled bolus (i.e., bolus duration) and thus enabling accurate perfusion quantification (Fig. 1A) [20, 24].

Continuous/pseudo-continuous arterial spin labeling (CASL/pCASL)

CASL involves the use of a constant RF pulse along with a selective gradient for longer durations to invert the inflowing blood upstream of the imaging region of interest. CASL has improved SNR compared to PASL since CASL enables inverting the inflowing blood for longer durations [25]. However, performing continuous RF pulses for prolonged durations is challenging on commercially available whole-body MR scanners. To overcome this hardware limitation, the pseudo-continuous ASL scheme was developed as an alternative to CASL [22]. In pCASL, a labeling plane is generated by a train of short RF pulses that mimics a continuous RF pulse played-out simultaneously with a slice-selective gradient (Fig. 1B). The inflowing spins crossing the labeling plane are inverted following the adiabatic fast passage [26]. After a given post-label delay (PLD), the labeled blood perfuses into the imaging region. Phase-cycled RF pulses are applied in the control condition to mitigate the differences between the control and the labeled image due to magnetization transfer (MT) effects. There are two variations of pCASL, namely balanced and unbalanced schemes [27]. The key difference between the two variants lies in the mean gradient: in the balanced pCASL, the mean gradient is non-zero and remains the same for the label and the control schemes, while for the unbalanced pCASL, the mean gradient is 0 in the control scheme. The unbalanced pCASL has demonstrated greater robustness to off-resonance effects [28], and is typically preferred in the body applications.
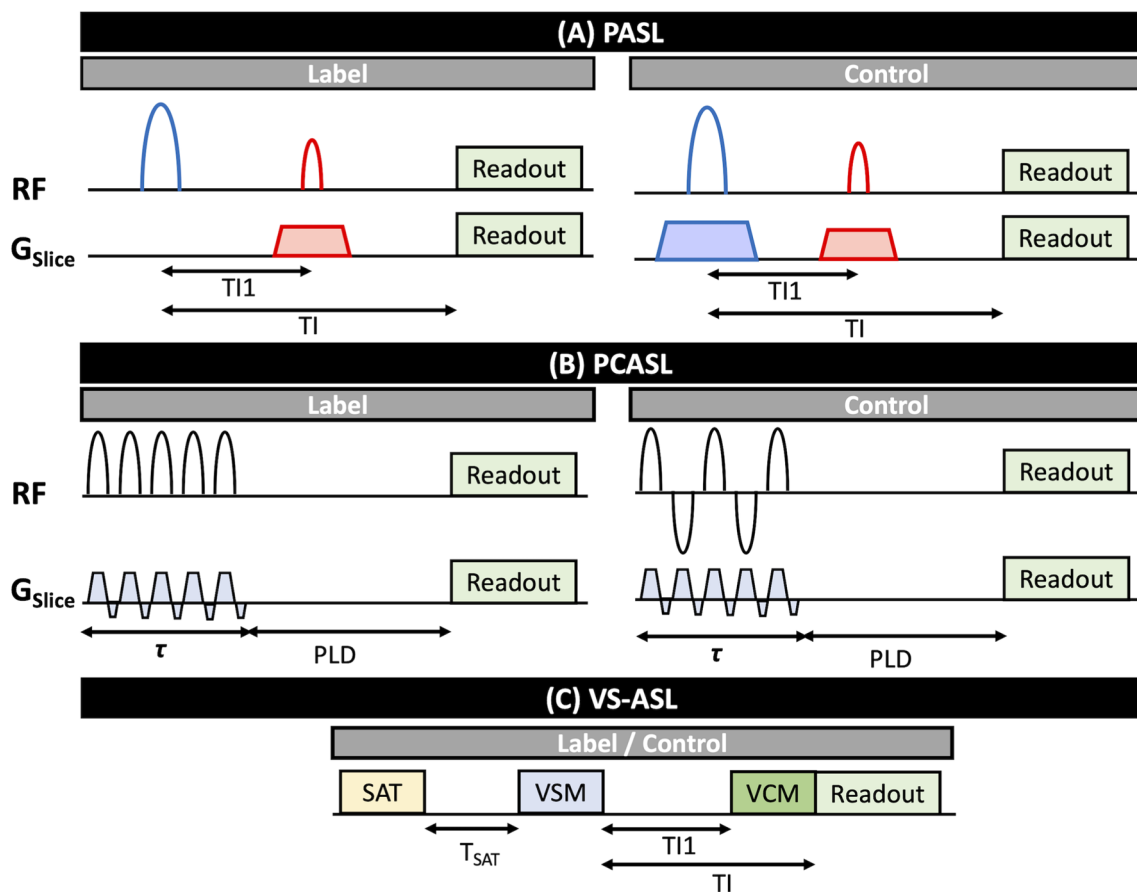
Fig. 1 Schematics of commonly used ASL pulse sequences along with their timing definitions. **A** Pulsed ASL (PASL) using FAIR: Non-selective and selective RF pulses are depicted in blue for the label and control schemes, respectively. Inflow saturation pulses are shown in red. TI1 and TI represent the bolus duration and the inversion time, respectively. **B** Pseudo-continuous ASL (pCASL): For the label condition, a train of RF pulses is used to induce a flow-driven adiabatic inversion in a labeling plane. For the control condition, the phase of the RF pulses is alternated such that no inversion is achieved. τ represents the labeling duration, and PLD denotes the post-label delay. **C** Velocity-selective ASL (VS-ASL): For both the control and the label schemes, three modules are played out before signal readout: pre-saturation module (SAT), velocity-selective module (VSM), and vascular-crusher module (VCM). Here, TI1 also represents the bolus duration, T_{SAT} is the time between SAT and VSM, and TI is the time between VSM and readout

Velocity-selective arterial spin labeling (VS-ASL)

VS-ASL is a method that labels arterial blood based on its flow velocity, making this technique insensitive to variations in arterial transit times. In VS-ASL, a specific cut-off velocity (V_c) is chosen and all spins flowing above this velocity are labeled [23]. VS-ASL pulse sequence consists of three primary modules: pre-saturation module (SAT), velocity-selective module (VSM), and vascular crushing module (VCM) (Fig. 1C). There are two variants for the VSM, which are based on either saturation pulses or inversion pulses. In VS-ASL, RF pulses are the same for the label and the control scheme; however, flow-sensitive gradients are either played out solely during the acquisition of the labeled image, or flow-compensated during the acquisition of the control image [29]. VS-ASL was developed as an alternative to pCASL and PASL, due to its increased robustness to slow arterial transit times and its suitability for applications where selective labeling of the feeding vessels is challenging.

ASL perfusion quantification

One of the major advantages of ASL is its ability to generate quantitative perfusion measurements in physiological values of mL/100 g/min. ASL perfusion values can be calculated following the general kinetic model [30] using the perfusion difference image (ΔM), ASL labeling efficiency, longitudinal relaxation time of blood ($T1_{blood}$), and a proton density-weighted image (M_0). To quantify ASL perfusion, two primary models have been developed: a single-compartment model [30] and a two-compartment model [31, 32]. Due to its simplicity, the single-compartment model also known as the Buxton model, has been widely used and is mathematically described as:

$$\Delta M = 2 \cdot \alpha \cdot M_{0b} \cdot f \cdot \int_0^t c(t) \cdot r(t - \tau) \cdot m(t - \tau) d\tau, \quad (1)$$

where α is the labeling efficiency, M_{0b} is the equilibrium magnetization of blood, and f is perfusion. t and τ denote time and labeling duration, respectively. The delivery, residue, and magnetization relaxation functions are represented by $c(t)$, $r(t-\tau)$, and $m(t-\tau)$, respectively. This model is graphically depicted in Fig. 2.

To solve Eq. (1), the following assumptions are considered: (a) all labeled arterial blood is contained within the tissue voxel, (b) the presence of only one compartment connecting the tissue and the microvasculature, and (c) the total longitudinal relaxation is governed by TI_{blood} [33]. Under these assumptions, the solutions to quantify perfusion (f) for FAIR, pCASL, and VS-ASL are respectively defined as:

$$f_{\text{FAIR}} = \frac{\Delta M}{M_0} \cdot \frac{6000 \cdot \lambda}{2 \cdot \alpha \cdot TI1} \cdot e^{\frac{TI}{T1_{blood}}} [\text{mL}/100 \text{ g}/ \text{min}], \quad (2)$$

$$f_{\text{pCASL}} = \frac{\Delta M}{M_0} \cdot \frac{6000 \cdot \lambda}{2 \cdot \alpha \cdot T1_{blood}} \cdot \frac{e^{\frac{PLD}{T1_{blood}}}}{1 - e^{-\frac{\tau}{T1_{blood}}}} [\text{mL}/100 \text{ g}/ \text{min}], \quad (3)$$

$$f_{\text{VS-ASL}} = \frac{\Delta M}{M_0} \cdot \frac{6000 \cdot \lambda}{2 \cdot \alpha \cdot TI1} \cdot \frac{e^{\frac{TI}{T1_{blood}}}}{1 - e^{-\frac{T_{SAT}}{T1_{blood}}}} [\text{mL}/100 \text{ g}/ \text{min}] \quad (4)$$

where λ is the blood–tissue partition coefficient, TI and TI1 represent the inversion time and the arterial blood bolus duration, respectively (for FAIR); PLD is the post-labeling delay and τ is the labeling duration (for pCASL); T_{SAT} is the time between the end of the saturation pulses and the start of the VSM (for VS-ASL). The TI_{blood} is assumed to be 1.48 s at 1.5 T and 1.65 s at 3 T [34]. M_0 is the equilibrium magnetization of arterial blood, which is often measured using
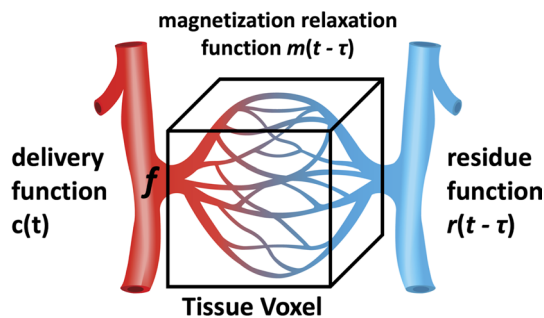

Fig. 2 Single-compartment model for ASL perfusion quantification. The delivery function $c(t)$ represents the labeled arterial blood that perfuses into the tissue voxel at a rate f. The magnetization relaxation function, $m(t-\tau)$, considers the effects of longitudinal relaxation of blood (TI_{blood}) at $t-\tau$, and the residue function, $r(t-\tau)$, reflects the wash-out of labeled blood from the tissue voxel at $t-\tau$

the proton density-weighted image using same acquisition parameters as the ASL image but without any labeling.

Methodological challenges of ASL in body applications

Continuous progress over the past three decades has overcome the limitations of ASL in the brain applications. The implementation of ASL in the chest and abdomen, however, is often obstructed by physiological motion, such as cardiac motion, respiratory motion, and peristalsis of gastrointestinal tracts. This is further worsened by increased sensitivity to B0 and B1 + field inhomogeneities, which are more pronounced in the body and at higher magnetic field strengths. The main source of B0 field inhomogeneities in the body is the presence of air in spaces such as alveoli in the lungs or in the intestines. On the other hand, the B1 + field inhomogeneities are influenced by size and shape of the body as well as tissue composition. The combined impact of these factors leads to reduced labeling efficiency, decreased SNR, and an increase in image artifacts. Nevertheless, ongoing technical advancements over the years have been dedicated to address these challenges for successful translation of ASL in body applications. Some of these advances are discussed below.

Image acquisition methods

Several strategies have been developed to acquire ASL images in the body, regardless of the specific labeling strategies. These include spin echo echo-planar imaging (SE-EPI), fast or turbo spin echo (FSE/TSE), gradient echo (GRE), balanced steady state free precession (bSSFP), and the combined gradient and spin echo (GraSE) imaging. The majority of ASL images in the body has been acquired as a single slice 2D image. Recent work has also demonstrated multi-slice 2D images as well as 3D images.

2D acquisitions

The majority of 2D acquisitions have primarily employed either SE-EPI [35] or single-shot TSE (SShTSE) [36] due to their fast acquisition times. Additionally, the use of a single excitation pulse with these sequences is particularly important due to its compatibility with background suppression (BGS), which is described in more detail below. Both SE-EPI and SShTSE acquisitions allow for an increased number of signal averages (NSAs), which is a crucial factor given that ASL images typically have low SNR and require multiple NSAs to achieve good image quality. While both SE-EPI and SShTSE acquisitions have been successfully demonstrated, each approach has its own set of advantages and disadvantages. For instance, SE-EPI images are more

prone to B0 inhomogeneities and suffer from geometric distortions, which can significantly affect the image quality. SShTSE images, on the other hand, are more robust to B0 inhomogeneities due to multiple refocusing pulses; however, these images often suffer from increased image blurring due to longer readout durations. Although parallel imaging methods, such as SENSE, GRAPPA, or Compressed Sense (CS), can be used to shorten the readout durations or reduce geometric distortions, they are often not recommended for ASL images because these acceleration methods tend to further reduce the SNR. SE-EPI and SShTSE have also been extended to acquire multiple 2D slices [37], albeit with slightly longer scan times. In specific cases, bSSFP has also been used to acquire 2D ASL images particularly for lung ASL studies [38].

3D acquisitions

There are several advantages in acquiring 3D ASL images compared to 2D images. First, 3D acquisitions enable volumetric coverage of the entire organ being imaged. Second, the increased number of slices achievable with 3D acquisition allow volumetric coverage with similar SNR in the same acquisition time instead of the higher NSAs with 2D acquisition. Third, the nature of volumetric excitation in 3D acquisitions makes them well-suited for BGS pulses, ensuring uniform background suppression throughout the volume. However, achieving good image quality with 3D acquisition has its own challenges. The majority of 3D acquisitions in body applications use either 3D rapid acquisition with relaxation enhancement (RARE) [39, 40], also known as FSE/TSE, or 3D GraSE [41]. A major challenge of these techniques is image blurring caused by T2 and T2* decay due to longer echo trains used to acquire the combined phase and slice encodes in the volume. Furthermore, 3D GraSE acquisitions are sensitive to field inhomogeneities, which are more pronounced in the body and cause image distortions. For FSE/TSE acquisitions, higher specific absorption rates (SAR) due to multiple refocusing pulses that causes high-power deposition is a concern [42]. Addressing these challenges are currently an active area of research and further developments are needed before the routine use of 3D acquisitions for volumetric ASL imaging in the body [43].

Post label delay (PLD)

During TI (FAIR/VS-ASL) or PLD (pCASL), two critical processes occur. First, the labeled blood perfuses into the tissue. Second, the labeled blood also recovers to its full magnetization. Thus, the TI/PLD is chosen at an optimal time that strikes a balance between being long enough to flow into the tissue but also short enough such that the blood is not completely recovered to its full magnetization. During this TI/PLD, two important functionalities are incorporated for successful quantitative ASL measurements and minimize artifacts: background suppression and inflow saturation.

Background suppression (BGS)

It is well-recognized that a single inversion pulse nulls the signal from a single tissue based on its *T1* relaxation time. For example, STIR nulls the fat signal with a short TI of 150–200 ms, while FLAIR nulls cerebrospinal fluid (CSF) with a long TI of ~2200 ms at 3 T. Similarly, the application of 4–5 inversion pulses with optimal TIs can suppress signals from tissues across a broad range of *T1* relaxation times [44]. Based on this principle, the signal intensities of the static tissue between the control and the labeled images can be sufficiently suppressed using pairs of inversion pulses. Typically, either 2 or 4 BGS pulses are utilized to substantially decrease the signal from the static background tissue, without affecting the signal difference between the control and the labeled image. The application of BGS pulses improves the image quality considerably and is highly recommended for ASL in body applications [36, 45].

Inflow saturation

During TI/PLD, it is important to note that fresh blood continues to flow even after the labeling has ended. This fresh blood often tends to accumulate in the major vessels due to shorter transit time and does not contribute to the perfusion signal in that specific tissue. While this signal in the major vasculature should ideally be identical between the control and the labeled images, it often differs due to variations in the cardiac cycle and the transit delays. To address this, inflow saturation pulses are applied upstream to the imaging region of interest during TI/PLD to suppress the signal from the fresh inflowing blood. The inflow saturation pulses also help define the bolus width of pulsed labeling such as FAIR. This can be achieved using schemes such as QUIPPS II saturation or Q2-TIPS [46] and enables quantitative perfusion measurements [47].

Post-processing methods

Perfusion-weighted images are typically generated by subtracting the control and the labeled images. Certain retrospective methods can be employed to improve the image quality during this process. (1) To address the inherently low SNR of ASL images, signal averaging can be performed on a voxel-wise basis across multiple control-label measurements. This technique not only improves SNR but also provides a degree of robustness against motion artifacts, particularly when images are acquired using respiratory-triggering or guided-breathing

approaches [36]. (2) Another method would be to identify and either remove or assign lower weights to outlier measurements. Outliers are often misaligned with the majority of the images and can negatively impact the subtraction process. By minimizing their effect, the overall image quality can be improved. (3) Retrospective sorting of images can be performed using data from external sensors such as respiratory bellows. This sorting helps align images according to respiratory or other physiological cycles, reducing motion-related artifacts [48]. These post-processing steps help reduce image artifacts, reduce partial volume effects, and improve the SNR of the perfusion-weighted signal and the repeatability of perfusion measurements. Importantly, these methods should not only be applied to align ASL control and labeled images but also to align the corresponding M_0 images, which are essential for accurate perfusion quantification.

Quantitative ASL-MRI in highly perfused organs in the body

In this section, we have summarized potential clinical applications, challenges, and state-of-the-art ASL methods to quantify perfusion in some of the highly perfused organs in the thorax (lungs), abdomen (kidneys, liver, pancreas), and pelvis (placenta) of the human body. Table 1 summarizes the ASL applications in the body, including common readouts, disease focus, technical challenges, and literature footprint.

Lungs

Clinical applications

The lungs play a critical role in the delivery of oxygen and removal of carbon dioxide, and the perfusion is essential for this function. Lung is distinct from other organs since the lung perfusion is achieved through deoxygenated blood from

Table 1 ASL applications in the body

Anatomy of interest	Common readout	Disease focus	Technical challenges	Literature footprint*	International consensus
Lungs	SShTSE or bSSFP	Pulmonary embolism, obstructive pulmonary disease, pulmonary hypertension, emphysema, interstitial lung disease, and cystic fibrosis	• B0 inhomogeneities caused by air/tissue interfaces • Highly pulsatile blood flow • Complex anatomy • Low SNR due to low proton density • Cardiac and respiratory motion	<65	No
Kidneys	SE-EPI, SShTSE, 3D TSE or 3D GraSE	Chronic kidney disease, acute kidney injury, diabetes, hypertension, lupus nephritis, renovascular disease, renal transplants, and renal cancer	• B0 and B1 inhomogeneities caused by the proximity to the lungs • Respiratory motion • Measurement of perfusion in the medulla is challenging due to lower flow and longer arterial transit times compared to the cortex	>250	Yes [43]
Liver	EPI	Cirrhosis, portal hypertension, and monitoring the response to liver tumor treatments	• Respiratory motion • Dual blood supply: 70–75% from the portal vein and 25–30% from the hepatic artery	<30	No
Pancreas	bSSFP or SShTSE	Diabetes, chronic pancreatitis, and pancreatic cancer	• B0 inhomogeneities caused by large air pockets in the surrounding bowels • Peristaltic and respiratory motion • Multiple blood supply • Short *T1*	<10	No
Placenta	SShTSE or 3D GraSE	Chronic hypertension, and in pregnancies with congenital heart disease	• Multiple arterial blood supply • Complex anatomy • B1 and B0 inhomogeneities caused by the amniotic fluid	<20	No

*Number of published articles found in PubMed

the right ventricle of the heart. ASL can measure quantitative perfusion without the need for exogenous contrast agent and also avoids ionizing radiation compared to existing lung perfusion imaging methods, such as planar scintigraphy and contrast-enhanced computed tomography. This is particularly advantageous for longitudinal monitoring, especially in younger and pediatric patients. ASL measured perfusion in lungs is an emerging area of research with potential clinical implications in various lung conditions including pulmonary embolism (PE), chronic obstructive pulmonary disease, pulmonary hypertension, emphysema, interstitial lung disease, and cystic fibrosis.

Challenges

ASL perfusion imaging in the lungs is exceptionally challenging due to multiple factors. The air/tissue interfaces in the lungs cause high B0 field inhomogeneities impacting the labeling efficiency and susceptibility-induced signal loss, especially with SE-EPI and bSSFP acquisitions. The highly pulsatile blood flow in the pulmonary arteries combined with the complex anatomy makes it difficult for achieving high labeling efficiency. Further, the low proton density of the lungs coupled with cardiac and respiratory motion contributes to low SNR.

Methodological state-of-the-art

Lung ASL perfusion imaging is still a predominantly research focused area. Due to the aforementioned challenges, most lung ASL studies have been performed at 1.5 T or lower field strengths using FAIR labeling [49] and SShTSE readout [50]. The higher sensitivity to cardiac motion necessitates the use of cardiac gating for data acquisition, especially with SShTSE sequences [51]. The implementation of BGS has enabled multi-slice acquisitions during free

breathing using FAIR to cover the entire lungs in <5 min of acquisition time with demonstrated clinical utility in PE [52]. Recent technical advancements have also made it possible to use pCASL labeling of right or left pulmonary arteries and the measurement of lung perfusion using either SShTSE (Fig. 3) [51] or bSSFP acquisitions [53, 54].

Kidneys

Clinical applications

Assessment of kidney function is critical for effective management in clinical care, and glomerular filtration rate (GFR) is considered the gold standard measurement [55]. However, GFR provides a global measure of the kidney function and is suboptimal to detect local lesions or dysfunction as observed in tumors, ischemia, or sepsis. Many kidney diseases including chronic kidney disease (CKD) and acute kidney injury (AKI), involve impaired kidney function and hence are often contraindicated for use of GBCAs due to potential risks [56]. Therefore, ASL measured non-contrast perfusion serves as a safe and reliable alternative method for the assessment of kidney function. Renal ASL has been applied across a variety of kidney diseases including CKD, AKI, diabetes, hypertension, lupus nephritis, renovascular disease, renal transplants, and renal cancer [57].

Challenges

Several factors pose risk for successful ASL measurements in the kidneys, which include B0 and B1 field inhomogeneities, along with motion. Motion is a common challenge across all labeling strategies; however, B0 and B1 field inhomogeneities are particularly problematic for pCASL due to the proximity of labeling to the lungs [58, 59]. While 3D pCASL has the potential to achieve whole-kidney coverage,

Fig. 3 Individual dynamics of perfusion-weighted lung ASL images acquired in a volunteer using cardiac-triggered pCASL labeling of right pulmonary artery and BGS (top row) and the corresponding perfusion-weighted images acquired using FAIR (bottom row). The quantified perfusion maps from the three signal averages show similar values between the two labeling schemes, with each approach acquired in an 18 s breathhold. Reproduced from ref. [51] with permission from Elsevier
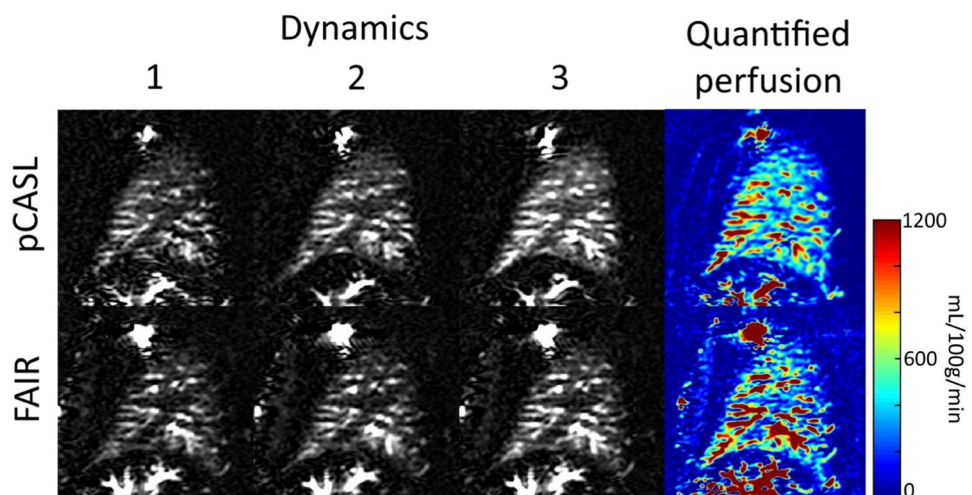
it suffers from reduced labeling efficiency leading to lower SNR or complete signal loss in some cases [60]. On the other hand, labeling with FAIR is more robust but is often restricted to 2D images due to the inclusion of aorta only in the label image but not in the control image. This constrains the labeling slab coverage and thus the field-of-view coverage in the slice orientation (Fig. 4). An additional challenge is the reliable measurement of perfusion in the medulla as it exhibits lower flow and longer transit times compared to the renal cortex. This results in both reduced SNR and partial volume contamination with the cortical perfusion signal.

Methodological state-of-the-art

Outside of brain, the majority of ASL development has been focused on kidney imaging given its higher perfusion. Based on the recommendations of PARENCHIMA [61], both FAIR and pCASL are considered optimal labeling strategies for the assessment of kidney perfusion [43]. SE-EPI and SShTSE acquisitions are commonly used, often with multiple signal averages and with BGS to achieve sufficient SNR (Fig. 4).

While substantial progress has been made in achieving volumetric coverage of whole kidneys, 3D ASL of kidneys is still a challenging endeavor. Current methods are matured to measure renal cortical perfusion, and further research is needed to improve the measurement of medullary perfusion with greater confidence.

Liver

Clinical applications

The liver is a vital abdominal organ involved in various metabolic functions. Abnormal blood flow in the liver has been observed in a wide spectrum of hepatic diseases including cirrhosis, hepatocellular carcinoma, hemangiomas, metastatic disease, liver transplantation, and cholangiocarcinoma [62]. While contrast-enhanced imaging methods can reliably detect perfusion abnormalities in the liver, they are often contraindicated in patients with kidney dysfunction, a common comorbid condition seen in advanced liver diseases [63]. ASL offers a promising alternative for assessing
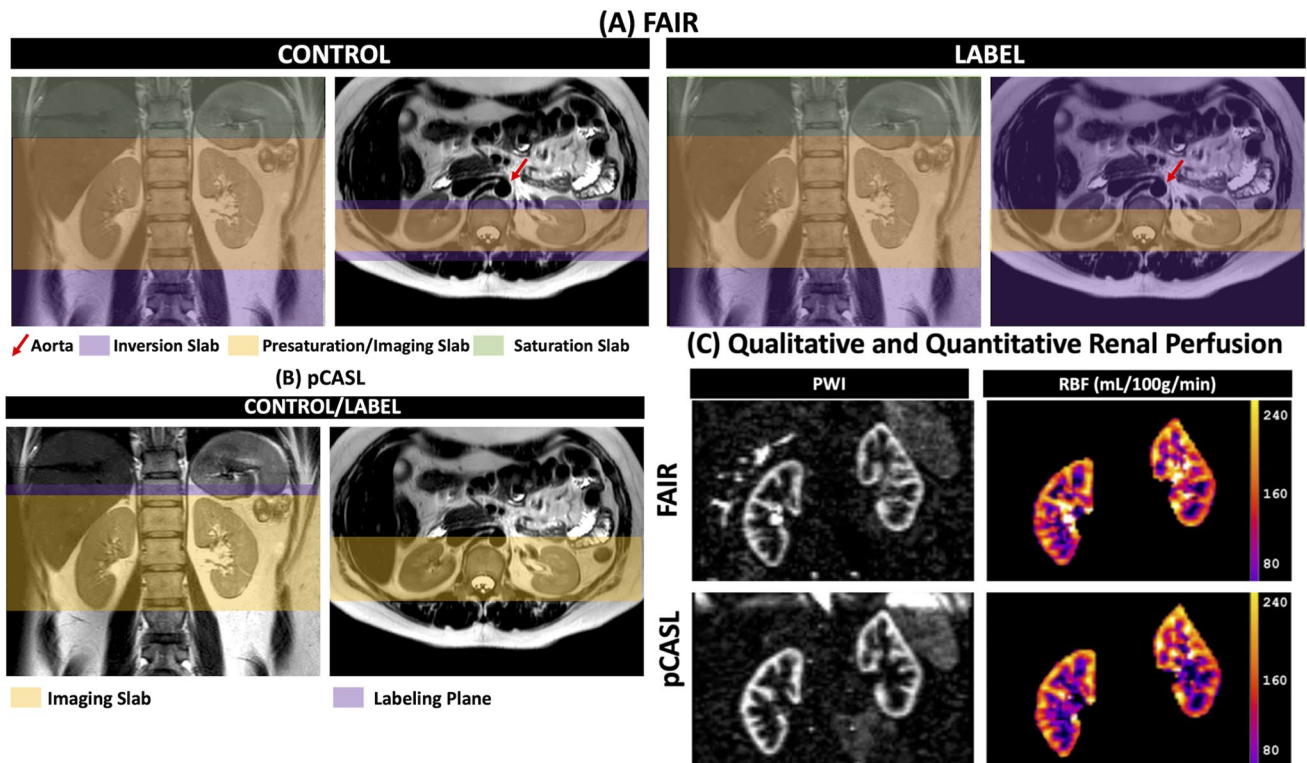

Fig. 4 Top row (**A**) FAIR labeling scheme for kidneys. In the control scheme, the inversion pulse (purple slab) is applied in the imaging region (orange slab) without overlapping the aorta (indicated by red arrow) in the axial plane; for the label scheme a non-selective inversion pulse is applied. Given the proximity of the aorta to kidneys, full coverage is challenging to achieve with FAIR. Bottom left (**B**) pCASL labeling scheme for kidneys. The labeling plane (purple) is applied axially across the abdominal aorta for both control and label schemes and the imaging slab (orange) can cover the entire kidneys. Bottom right (**C**) examples of perfusion-weighted images (PWI) and quantitative renal blood flow (RBF) maps acquired in a healthy volunteer using FAIR (top) and pCASL (bottom). The PWI and RBF maps were reproduced from the open source article Nery F et. al. [43] under the Creative Commons CC BY license

liver perfusion and has shown initial feasibility in evaluating conditions, such as cirrhosis [64], portal hypertension [65], and monitoring the response to liver tumor treatments [66].

Challenges

Liver has a remarkable dual blood supply with 70–75% from the portal vein and the remaining 25–30% from the hepatic artery [67]. This creates a challenge for ASL in positioning the labeling planes to independently assess the contributions from portal vein and the hepatic artery (Fig. 5, top left) [68]. Alternative methods include combining FAIR and pCASL (Fig. 5, top middle), or careful placement of the pCASL labeling plane covering both portal vein and hepatic artery (Fig. 5, top right) can generate global liver perfusion images [69, 70]. However, the placement of the labeling plane is sensitive to breathing motion, which is a major source of artifacts in liver ASL imaging.

Methodological state-of-the-art

The majority of liver ASL studies were performed using FAIR labeling to circumvent the challenges associated

with dual blood supply. pCASL labeling with multiple PLDs have also been successfully used to measure liver perfusion along with blood transit times within clinically feasible scan times [71]. Ongoing efforts have focused on developing free-breathing protocols and incorporating various motion correction algorithms. For example, a promising motion-compensation technique using 2D-EPI navigators has been implemented in a 3D pCASL sequence [69]. Despite these developments, liver ASL imaging remains primarily a research tool and is not yet widely adopted in clinical practice.

Pancreas

Clinical applications

Pancreas plays a critical role in producing hormones that are responsible for regulating blood sugar levels (endocrine system) as well as enzymes that are implicated in maintaining digestive functions (exocrine system). Hence, measuring pancreatic perfusion can be highly valuable in various conditions, such as diabetes, chronic pancreatitis, and pancreatic cancer. Few research groups have used ASL to study the
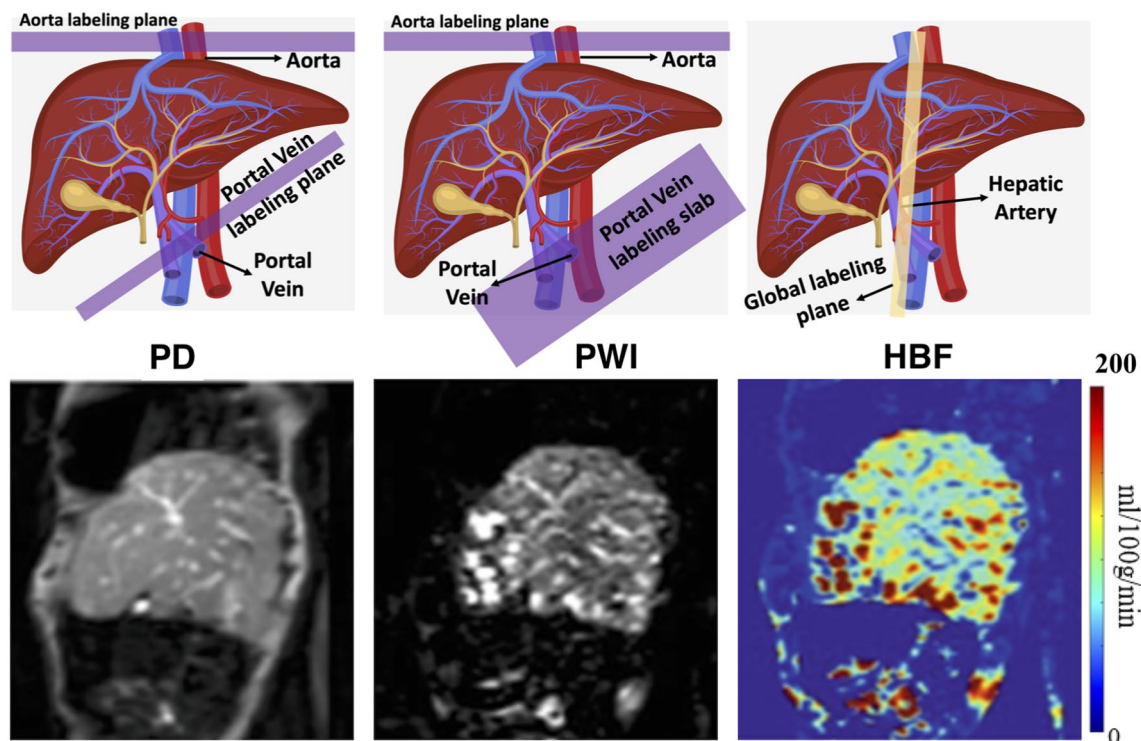

Fig. 5 Top row: Liver labeling schemes. Left: pCASL labeling scheme with two labeling planes to independently label the aorta and the portal vein. Middle: Combined PASL and pCASL scheme to selectively label the portal vein and the aorta, respectively. Right: pCASL scheme with careful placement of labeling plane to label both the hepatic artery and the portal vein. Bottom row: Liver proton density-weighted image (PD), perfusion-weighted image (PWI), and hepatic blood flow (HBF) map acquired with a pCASL-EPI sequence with BGS at 3 T. Figure in the bottom row was reproduced from ref. [17] with permission from John Wiley & Sons with some modifications

pancreatic blood flow by modulating with either intravenous secretin to stimulate endocrine secretions [72] or glucose to stimulate exocrine secretions [73] and observed increased perfusion in response to the modulators. Given that the applications of ASL in the pancreas are nascent, there are only limited studies in the literature demonstrating the clinical applications.

Challenges

The major challenges associated with pancreatic ASL imaging are the presence of large air pockets in the surrounding bowels, which lead to strong B0 field inhomogeneities. Additionally, peristaltic and respiratory motion can further complicate ASL imaging. Further, the arterial supply to different parts of the pancreas (head, body, and tail) originates from different branches of superior mesenteric artery and splenic artery, making it challenging to assess perfusion in different regions of the pancreas. Moreover, the *T1* relaxation times of pancreas are relatively short (584 ms at 1.5 T and 725 ms at 3 T) [74] and results in rapid signal decay during ASL experiment leading to reduced SNR.

Methodological state-of-the-art

Early studies in pancreatic ASL perfusion measurements were demonstrated using FAIR labeling and bSSFP acquisition in healthy volunteers at 1.5 T [75]. More recent work has used pCASL labeling with BGS and SShTSE readout to achieve pancreatic perfusion at 3 T due to its longer *T1* (Fig. 6) [73]. Nevertheless, additional development and optimization are warranted for routine use of ASL for the assessment of pancreatic perfusion.

Placenta

Clinical applications

The placenta is a temporary organ formed in the uterus during pregnancy, with key functions including the supply of oxygen and nutrients to the developing fetus, waste elimination, and support placental–fetal immunological functions. Conditions such as chronic hypertension that leads to intrauterine growth restriction and pre-eclampsia are associated with decreased placental perfusion [76]. Since the administration of GBCAs is contraindicated in pregnancy [77], ASL provides the non-contrast alternative imaging method to measure placental perfusion in vivo. ASL measured
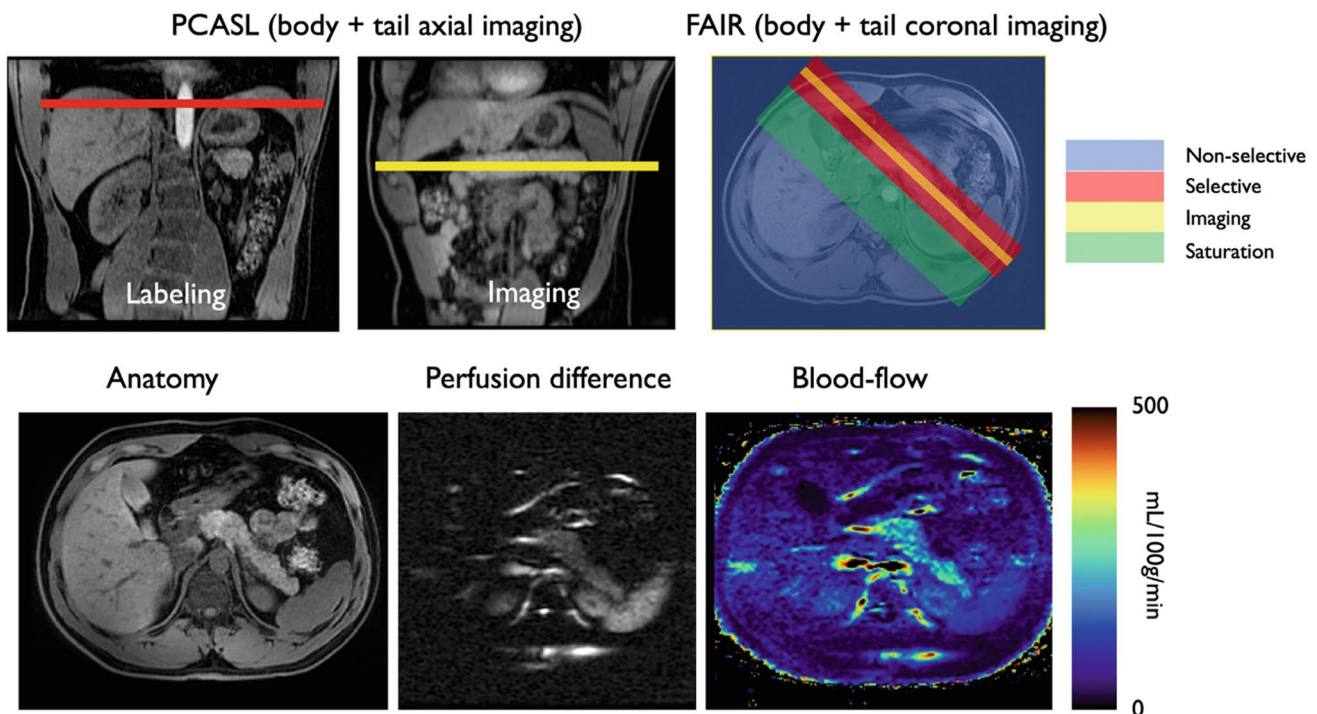

Fig. 6 Top row: Labeling geometry for pCASL and FAIR pancreatic perfusion imaging. Bottom row: Illustration of a dataset with anatomical, perfusion-weighted image, and pancreatic blood flow map in a healthy volunteer acquired using a pCASL-SShTSE sequence at 3 T. Reproduced from ref. [17] with permission from John Wiley & Sons

placental perfusion has been successfully demonstrated in healthy pregnancies [78], pregnancies impacted by chronic hypertension [79], and in pregnancies with congenital heart disease [80]. ASL offers a promising technique to assess placenta perfusion, helping to identify and address fetal development issues caused by inadequate blood supply.

Challenges

One of the major challenges in placental ASL is determining optimal labeling regions. On the maternal side, placenta receives blood flow from the descending aorta, internal iliac arteries, and uterine arteries. These arterial pathways are complex and makes it challenging for selective labeling. Furthermore, the shape and the location of the placenta also vary substantially across individuals, further complicating the labeling strategies. The presence of amniotic fluid further adds to the challenges by increasing both B1 and B0 field inhomogeneities, reducing the labeling efficiency and causing susceptibility-induced signal loss.

Methodological state-of-the-art

The initial demonstration of placental perfusion using ASL dates back two decades, using FAIR labeling and Look-Locker imaging on a single slice at 0.5 T [12]. The launch of Human Placenta Project (HPP) by the National Institute of Child Health and Human Development [81] has renewed interest in multiple placental ASL studies using advanced labeling strategies. Due to the complexities of placental vascular anatomy, pCASL labeling was performed at the descending aorta often above the aortic bifurcation to label all feeding vessels to the placenta [82]. This necessitates longer labeling and PLDs due to increased distance of the placenta from the labeling plane. Nevertheless, several studies have reported successful pCASL labeling for the assessment of placental perfusion (Fig. 7). VS-ASL addresses the challenges associated with selective labeling and has been successfully applied in normal pregnancies and pregnancies complicated by congenital heart disease [83].

Future directions

ASL perfusion imaging for body applications has made significant progress since its original development in early 1990s. While a substantial portion of ASL perfusion imaging research outside of the brain has focused on kidney perfusion, the quality of kidney ASL images can still vary among different research groups. Similar variations were also observed in cerebral perfusion during the early development, until the ASL community came together to collaborate and establish a consensus recommendation for brain ASL [33]. Similar efforts to standardize kidney ASL have been made through the PARENCHIMA consortium and resulted in guidelines for kidney ASL [43]. However, due to the technical challenges and variations among different implementations, further work is needed to improve the robustness of ASL for kidneys as well as for other body applications. It is worth noting that ASL has also been evaluated in several other clinically important

Fig. 7 T2-weighted images (left) and ASL perfusion map (right) acquired at the same imaging slice in a normal pregnant subject shown at 16 week (top row) and 28 week (bottom row) gestational ages (GA) respectively. The white dotted line outlines the placenta, drawn on the T2-weighted image and copied over to perfusion map. The arrows represent the vascular signal in the femoral arteries. The residual signal outside the placenta, particularly at 28 week gestational age, shows variations in the background signal. The placental blood flow at visit 1 (top row) was 140 ± 152 mL/100 g/min and at visit 2 (bottom row) was 70 ± 45 mL/100 g/min in this normal subject. Reproduced from ref. [79] with permission from Springer Nature
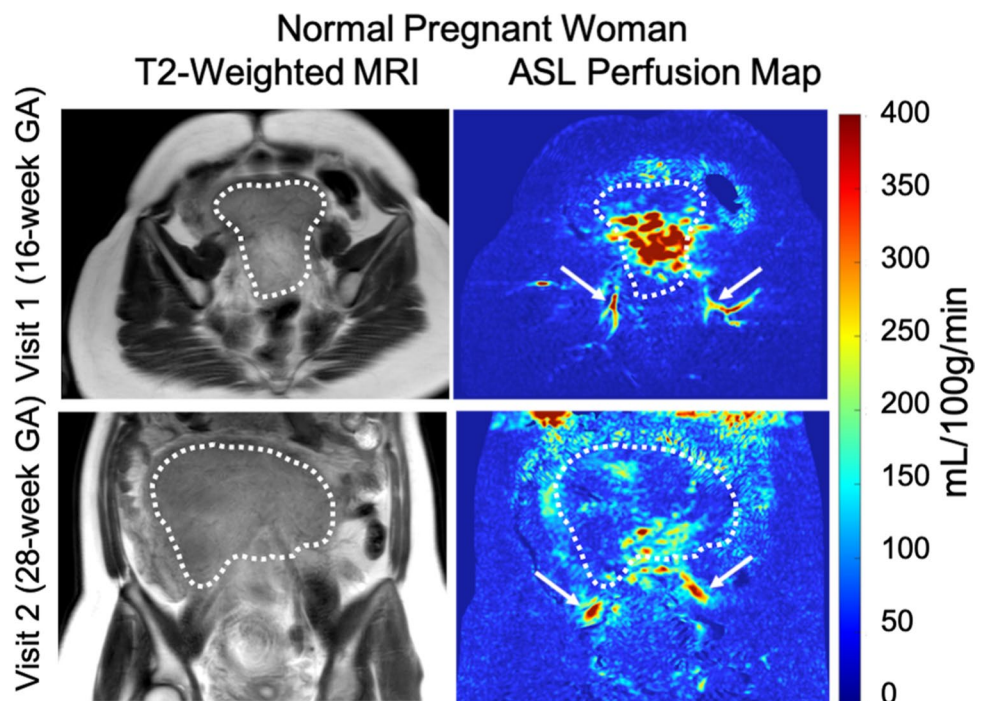
regions within the body including heart [84], spleen [85], prostate [86], and reproductive organs [87]. The emergence of artificial intelligence and machine learning holds great promise for improving the image quality of ASL perfusion imaging and enhancing the accuracy of perfusion quantification in various body regions [16]. Additional efforts are also being pursued to improve the accuracy of ASL blood flow quantification using new labeling strategies such as DiSpect [88] and novel quantification methods such as Quantitative Transport Mapping (QTM) [89]. These advanced techniques may play a significant role in propelling the field of ASL and expanding its clinical applications.

Moreover, advanced methods, such as diffusion-weighted ASL (DW-ASL) [90] and MR-Fingerprinting (MRF-ASL) [91], have the potential to estimate additional hemodynamic parameters accounting for microstructural characteristics. For example, DW-ASL has been previously used in the brain to estimate capillary permeability [92, 93]. Interestingly, this technique has been extended to kidneys for successful measurement of the glomerular blood transfer rate [94]. While some of these advanced ASL variants may not have been extensively explored outside the brain or validated in the existing body of literature, their applications look promising and can leverage the applicability of ASL in other organs and in the clinical setting.

Conclusion

ASL has evolved as a powerful tool for quantitative non-contrast perfusion imaging across multiple organs, offering insights into physiological and pathological processes. The non-invasiveness and quantitative nature of ASL makes it an attractive tool for clinical research and patient care. Continued advancements in ASL technology and its clinical translation hold promise for its broader integration into routine clinical practice, revolutionizing the diagnosis and management of various diseases.

Declarations

References

1. Bammer R, Amukotuwa SA (2024) Dynamic susceptibility contrast perfusion, part 1: the fundamentals. Magn Reson Imaging Clin N Am 32(1):1–23
2. Li X, Huang W, Holmes JH (2024) Dynamic contrast-enhanced (DCE) MRI. Magn Reson Imaging Clin N Am 32(1):47–61
3. Bell LC, Semmineh N, An H, Eldeniz C, Wahl R, Schmainda KM, Prah MA, Erickson BJ, Korfiatis P, Wu C, Sorace AG, Yankeelov TE, Rutledge N, Chenevert TL, Malyarenko D, Liu Y, Brenner A, Hu LS, Zhou Y, Boxerman JL, Yen YF, Kalpathy-Cramer J, Beers AL, Muzi M, Madhuranthakam AJ, Pinho M, Johnson B, Quarles CC (2019) Evaluating multisite rCBV consistency from DSC-MRI imaging protocols and postprocessing software across the NCI quantitative imaging network sites using a digital reference object (DRO). Tomography 5(1):110–117
4. Bell LC, Semmineh N, An H, Eldeniz C, Wahl R, Schmainda KM, Prah MA, Erickson BJ, Korfiatis P, Wu C, Sorace AG, Yankeelov TE, Rutledge N, Chenevert TL, Malyarenko D, Liu Y, Brenner A, Hu LS, Zhou Y, Boxerman JL, Yen YF, Kalpathy-Cramer J, Beers AL, Muzi M, Madhuranthakam AJ, Pinho M, Johnson B, Quarles CC (2020) Evaluating the use of rCBV as a tumor grade and treatment response classifier across NCI quantitative imaging network sites: part II of the DSC-MRI digital reference object (DRO) challenge. Tomography 6(2):203–208
5. Roberts DR, Lindhorst SM, Welsh CT, Maravilla KR, Herring MN, Braun KA, Thiers BH, Davis WC (2016) High levels of gadolinium deposition in the skin of a patient with normal renal function. Invest Radiol 51(5):280–289
6. McDonald RJ, McDonald JS, Kallmes DF, Jentoft ME, Murray DL, Thielen KR, Williamson EE, Eckel LJ (2015) Intracranial gadolinium deposition after contrast-enhanced MR imaging. Radiology 275(3):772–782
7. McDonald RJ, Levine D, Weinreb J, Kanal E, Davenport MS, Ellis JH, Jacobs PM, Lenkinski RE, Maravilla KR, Prince MR, Rowley HA, Tweedle MF, Kressel HY (2018) Gadolinium retention: a research roadmap from the 2018 NIH/ACR/RSNA workshop on gadolinium chelates. Radiology 289(2):517–534
8. Williams DS, Detre JA, Leigh JS, Koretsky AP (1992) Magnetic resonance imaging of perfusion using spin inversion of arterial water. Proc Natl Acad Sci U S A 89(1):212–216
9. Detre JA, Leigh JS, Williams DS, Koretsky AP (1992) Perfusion imaging. Magn Reson Med 23(1):37–45
10. Roberts DA, Detre JA, Bolinger L, Insko EK, Leigh JS Jr (1994) Quantitative magnetic resonance imaging of human brain perfusion at 1.5 T using steady-state inversion of arterial water. Proc Natl Acad Sci U S A 91(1):33–37
11. Roberts DA, Detre JA, Bolinger L, Insko EK, Lenkinski RE, Pentecost MJ, Leigh JS Jr (1995) Renal perfusion in humans: MR imaging with spin tagging of arterial water. Radiology 196(1):281–286
12. Gowland PA, Francis ST, Duncan KR, Freeman AJ, Issa B, Moore RJ, Bowtell RW, Baker PN, Johnson IR, Worthington BS (1998) In vivo perfusion measurements in the human placenta using echo planar imaging at 0.5 T. Magn Reson Med 40(3):467–473
13. Gach HM, Li T, J.C. L-T, Kam AW (2002) Liver perfusion MRI using arterial spin labeling. Paper presented at the Proceedings of the 10th ISMRM annual Meeting, Honolulu, HI, USA,
14. Qiu M, Wang J, Pinus A, Kim H, Constable RT (2006) Arterial spin labeling TrueFISP pancreas/liver perfusion imaging at 1.5 tesla. Paper presented at the Proceedings of the 14th ISMRM Annual Meeting, Seattle, WA, USA,
15. Mai VM, Berr SS (1999) MR perfusion imaging of pulmonary parenchyma using pulsed arterial spin labeling techniques: FAIRER and FAIR. J Magn Reson Imaging 9(3):483–487

16. Hernandez-Garcia L, Aramendia-Vidaurreta V, Bolar DS, Dai W, Fernandez-Seara MA, Guo J, Madhuranthakam AJ, Mutsaerts H, Petr J, Qin Q, Schollenberger J, Suzuki Y, Taso M, Thomas DL, van Osch MJP, Woods J, Zhao MY, Yan L, Wang Z, Zhao L, Okell TW (2022) Recent technical developments in ASL: a review of the state of the art. Magn Reson Med 88(5):2021–2042

17. Taso M, Aramendia-Vidaurreta V, Englund EK, Francis S, Franklin S, Madhuranthakam AJ, Martirosian P, Nayak KS, Qin Q, Shao X, Thomas DL, Zun Z, Fernandez-Seara MA, Group IPS (2023) Update on state-of-the-art for arterial spin labeling (ASL) human perfusion imaging outside of the brain. Magn Reson Med 89(5):1754–1776

18. Edelman RR, Siewert B, Darby DG, Thangaraj V, Nobre AC, Mesulam MM, Warach S (1994) Qualitative mapping of cerebral blood flow and functional localization with echo-planar MR imaging and signal targeting with alternating radio frequency. Radiology 192(2):513–520

19. Kwong KK, Chesler DA, Weisskoff RM, Donahue KM, Davis TL, Ostergaard L, Campbell TA, Rosen BR (1995) MR perfusion studies with T1-weighted echo planar imaging. Magn Reson Med 34(6):878–887

20. Kim SG (1995) Quantification of relative cerebral blood flow change by flow-sensitive alternating inversion recovery (FAIR) technique: application to functional mapping. Magn Reson Med 34(3):293–301

21. Wong EC, Buxton RB, Frank LR (1997) Implementation of quantitative perfusion imaging techniques for functional brain mapping using pulsed arterial spin labeling. NMR Biomed 10(4–5):237–249

22. Dai W, Garcia D, de Bazelaire C, Alsop DC (2008) Continuous flow-driven inversion for arterial spin labeling using pulsed radio frequency and gradient fields. Magn Reson Med 60(6):1488–1497

23. Wong EC, Cronin M, Wu WC, Inglis B, Frank LR, Liu TT (2006) Velocity-selective arterial spin labeling. Magn Reson Med 55(6):1334–1341

24. Wong EC, Buxton RB, Frank LR (1998) Quantitative imaging of perfusion using a single subtraction (QUIPSS and QUIPSS II). Magn Reson Med 39(5):702–708

25. Wolf RL, Wang J, Wang S, Melhem ER, O'Rourke DM, Judy KD, Detre JA (2005) Grading of CNS neoplasms using continuous arterial spin labeled perfusion MR imaging at 3 tesla. J Magn Reson Imaging 22(4):475–482

26. Bernstein MA, King KF, Zhou XJ (2004) Handbook of MRI pulse sequences. Elsevier Science

27. Wu WC, Fernandez-Seara M, Detre JA, Wehrli FW, Wang J (2007) A theoretical and experimental investigation of the tagging efficiency of pseudocontinuous arterial spin labeling. Magn Reson Med 58(5):1020–1027

28. Zhao L, Vidorreta M, Soman S, Detre JA, Alsop DC (2017) Improving the robustness of pseudo-continuous arterial spin labeling to off-resonance and pulsatile flow velocity. Magn Reson Med 78(4):1342–1351

29. Qin Q, Alsop DC, Bolar DS, Hernandez-Garcia L, Meakin J, Liu D, Nayak KS, Schmid S, van Osch MJP, Wong EC, Woods JG, Zaharchuk G, Zhao MY, Zun Z, Guo J, Group ISS (2022) Velocity-selective arterial spin labeling perfusion MRI: a review of the state of the art and recommendations for clinical implementation. Magn Reson Med 88(4):1528–1547

30. Buxton RB, Frank LR, Wong EC, Siewert B, Warach S, Edelman RR (1998) A general kinetic model for quantitative perfusion imaging with arterial spin labeling. Magn Reson Med 40(3):383–396

31. Parkes LM (2005) Quantification of cerebral perfusion using arterial spin labeling: two-compartment models. J Magn Reson Imaging 22(6):732–736

32. Chappell MA, Woolrich MW, Kazan S, Jezzard P, Payne SJ, MacIntosh BJ (2013) Modeling dispersion in arterial spin labeling: validation using dynamic angiographic measurements. Magn Reson Med 69(2):563–570

33. Alsop DC, Detre JA, Golay X, Günther M, Hendrikse J, Hernandez-Garcia L, Lu H, MacIntosh BJ, Parkes LM, Smits M, van Osch MJP, Wang DJJ, Wong EC, Zaharchuk G (2015) Recommended implementation of arterial spin-labeled perfusion MRI for clinical applications: a consensus of the ISMRM perfusion study group and the European consortium for ASL in dementia. Magn Reson Med 73(1):102–116

34. Zhang X, Petersen ET, Ghariq E, De Vis JB, Webb AG, Teeuwisse WM, Hendrikse J, van Osch MJP (2013) In vivo blood T1 measurements at 1.5 T, 3 T, and 7 T. Magn Reson Med 70(4):1082–1086

35. Gardener AG, Francis ST (2010) Multislice perfusion of the kidneys using parallel imaging: image acquisition and analysis strategies. Magn Reson Med 63(6):1627–1636

36. Robson PM, Madhuranthakam AJ, Dai W, Pedrosa I, Rofsky NM, Alsop DC (2009) Strategies for reducing respiratory motion artifacts in renal perfusion imaging with arterial spin labeling. Magn Reson Med 61(6):1374–1387

37. Buchanan CE, Cox EF, Francis ST (2018) Evaluation of 2D imaging schemes for pulsed arterial spin labeling of the human kidney cortex. Diagnostics (Basel) 8(3):43

38. Martirosian P, Klose U, Mader I, Schick F (2004) FAIR true-FISP perfusion imaging of the kidneys. Magn Reson Med 51(2):353–361

39. Greer JS, Wang X, Wang Y, Pinho MC, Maldjian JA, Pedrosa I, Madhuranthakam AJ (2019) Robust pCASL perfusion imaging using a 3D Cartesian acquisition with spiral profile reordering (CASPR). Magn Reson Med 82(5):1713–1724

40. Robson PM, Madhuranthakam AJ, Smith MP, Sun MR, Dai W, Rofsky NM, Pedrosa I, Alsop DC (2016) Volumetric arterial spin-labeled perfusion imaging of the kidneys with a three-dimensional fast spin echo acquisition. Acad Radiol 23(2):144–154

41. Nery F, De Vita E, Clark CA, Gordon I, Thomas DL (2019) Robust kidney perfusion mapping in pediatric chronic kidney disease using single-shot 3D-GRASE ASL with optimized retrospective motion correction. Magn Reson Med 81(5):2972–2984

42. Hernandez-Garcia L, Aramendía-Vidaurreta V, Bolar DS, Dai W, Fernández-Seara MA, Guo J, Madhuranthakam AJ, Mutsaerts H, Petr J, Qin Q, Schollenberger J, Suzuki Y, Taso M, Thomas DL, van Osch MJP, Woods J, Zhao MY, Yan L, Wang Z, Zhao L, Okell TW (2022) Recent technical developments in ASL: a review of the state of the art. Magn Reson Med 88(5):2021–2042

43. Nery F, Buchanan CE, Harteveld AA, Odudu A, Bane O, Cox EF, Derlin K, Gach HM, Golay X, Gutberlet M, Laustsen C, Ljimani A, Madhuranthakam AJ, Pedrosa I, Prasad PV, Robson PM, Sharma K, Sourbron S, Taso M, Thomas DL, Wang DJJ, Zhang JL, Alsop DC, Fain SB, Francis ST, Fernandez-Seara MA (2020) Consensus-based technical recommendations for clinical translation of renal ASL MRI. MAGMA 33(1):141–161

44. Dixon WT, Sardashti M, Castillo M, Stomp GP (1991) Multiple inversion recovery reduces static tissue signal in angiograms. Magn Reson Med 18(2):257–268

45. Taso M, Guidon A, Alsop DC (2019) Influence of background suppression and retrospective realignment on free-breathing renal perfusion measurement using pseudo-continuous ASL. Magn Reson Med 81(4):2439–2449

46. Luh WM, Wong EC, Bandettini PA, Hyde JS (1999) QUIPSS II with thin-slice TI1 periodic saturation: a method for improving accuracy of quantitative perfusion imaging using pulsed arterial spin labeling. Magn Reson Med 41(6):1246–1254

47. Song R, Loeffler RB, Hillenbrand CM (2010) Improved renal perfusion measurement with a dual navigator-gated Q2TIPS fair technique. Magn Reson Med 64(5):1352–1359

48. Cox EF, Buchanan CE, Bradley CR, Prestwich B, Mahmoud H, Taal M, Selby NM, Francis ST (2017) Multiparametric renal magnetic resonance imaging: validation, interventions, and alterations in chronic kidney disease. Front Physiol 8:696

49. Martirosian P, Boss A, Fenchel M, Deimling M, Schafer J, Claussen CD, Schick F (2006) Quantitative lung perfusion mapping at 0.2 T using FAIR True-FISP MRI. Magn Reson Med 55(5):1065–1074

50. Henderson AC, Prisk GK, Levin DL, Hopkins SR, Buxton RB (2009) Characterizing pulmonary blood flow distribution measured using arterial spin labeling. NMR Biomed 22(10):1025–1035

51. Greer JS, Wang Y, Udayakumar D, Hussain T, Madhuranthakam AJ (2023) On the application of pseudo-continuous arterial spin labeled MRI for pulmonary perfusion imaging. Magn Reson Imaging 104:80–87

52. Greer JS, Gooty V, Tandon A, Greil G, Hussain T, Madhuranthakam AJ Non-contrast, free-breathing pulmonary perfusion imaging in pediatric patients with congenital heart disease using multi-slice FAIR at 1.5T. In: Proceedings of the 27th Annual Meeting of ISMRM, Montreal, Canada, 2019. p 2175.

53. Seith F, Pohmann R, Schwartz M, Kustner T, Othman AE, Kolb M, Scheffler K, Nikolaou K, Schick F, Martirosian P (2020) Imaging pulmonary blood flow using pseudocontinuous arterial spin labeling (PCASL) with balanced steady-state free-precession (bSSFP) readout at 1.5 T. J Magn Reson Imaging 52(6):1767–1782

54. Othman AE, Liang C, Komma Y, Munz M, Kolb M, Rath D, Guckel B, Pohmann R, Nikolaou K, Schwartz M, Kustner T, Martirosian P, Seith F (2023) Free-breathing arterial spin Labeling MRI for the detection of pulmonary embolism. Radiology 307(3):e221998

55. Boele-Schutte E, Gansevoort RT (2017) Measured GFR: not a gold, but a gold-plated standard. Nephrol Dialysis Transpl. https://doi.org/10.1093/ndt/gfw441

56. Grenier N, Cornelis F, Le Bras Y, Rigou G, Boutault JR, Bouzgarrou M (2013) Perfusion imaging in renal diseases. Diagn Interv Imaging 94(12):1313–1322

57. Odudu A, Nery F, Harteveld AA, Evans RG, Pendse D, Buchanan CE, Francis ST, Fernandez-Seara MA (2018) Arterial spin labelling MRI to measure renal perfusion: a systematic review and statement paper. Nephrol Dial Transpl. https://doi.org/10.1093/ndt/gfy180

58. Echeverria-Chasco R, Vidorreta M, Aramendia-Vidaurreta V, Cano D, Escalada J, Garcia-Fernandez N, Bastarrika G, Fernandez-Seara MA (2021) Optimization of pseudo-continuous arterial spin labeling for renal perfusion imaging. Magn Reson Med 85(3):1507–1521

59. Zhou L, Wang Y, Madhuranthakam AJ Improving the robustness of pseudo-continuous arterial spin labeling for renal perfusion imaging. In: Proceedings of the 29th Annual Meeting of ISMRM, Virtual, 2021. p 2539.

60. Greer JS, Wang Y, Pedrosa I, Madhuranthakam AJ (2019) Pseudo-continuous arterial spin labeled renal perfusion imaging at 3T with improved robustness to off-resonance. Paper presented at the International Society for Magnetic Resonance in Medicine (ISMRM), Montreal, Quebec, Canada,

61. Selby NM, Blankestijn PJ, Boor P, Combe C, Eckardt KU, Eikefjord E, Garcia-Fernandez N, Golay X, Gordon I, Grenier N, Hockings PD, Jensen JD, Joles JA, Kalra PA, Kramer BK, Mark PB, Mendichovszky IA, Nikolic O, Odudu A, Ong ACM, Ortiz A, Pruijm M, Remuzzi G, Rorvik J, de Seigneux S, Simms RJ, Slatinska J, Summers P, Taal MW, Thoeny HC, Vallee JP, Wolf

M, Caroli A, Sourbron S (2018) Magnetic resonance imaging biomarkers for chronic kidney disease: a position paper from the European cooperation in science and technology action PARENCHIMA. Nephrol Dial Transpl. https://doi.org/10.1093/ndt/gfy152

62. Oğul H, Kantarcı M, Genç B, Pirimoğlu B, Cullu N, Kızrak Y, Yılmaz O, Karabulut N (2014) Perfusion CT imaging of the liver: review of clinical applications. Diagn Interv Radiol 20(5):379–389

63. Cullaro G, Kanduri SR, Velez JCQ (2022) Acute kidney injury in patients with liver disease. Clin J Am Soc Nephrol 17(11):1674–1684

64. Bradley CR, Cox EF, Scott RA, James MW, Kaye P, Aithal GP, Francis ST, Guha IN (2018) Multi-organ assessment of compensated cirrhosis patients using quantitative magnetic resonance imaging. J Hepatol 69(5):1015–1024

65. Palaniyappan N, Cox E, Bradley C, Scott R, Austin A, O'Neill R, Ramjas G, Travis S, White H, Singh R, Thurley P, Guha IN, Francis S, Aithal GP (2016) Non-invasive assessment of portal hypertension using quantitative magnetic resonance imaging. J Hepatol 65(6):1131–1139

66. Johnson SP, Ramasawmy R, Campbell-Washburn AE, Wells JA, Robson M, Rajkumar V, Lythgoe MF, Pedley RB, Walker-Samuel S (2016) Acute changes in liver tumour perfusion measured non-invasively with arterial spin labelling. Br J Cancer 114(8):897–904

67. Kalra A, Yetiskul E, Wehrle CJ (2023) ([Updated 2023 May 1]) Physiology liver. StatPearls Publishing, Treasure Island (FL)

68. Pan X, Qian T, Fernandez-Seara MA, Smith RX, Li K, Ying K, Sung K, Wang DJJ (2016) Quantification of liver perfusion using multidelay pseudocontinuous arterial spin labeling. J Magn Reson Imaging 43(5):1046–1054

69. Huber J, Günther M, Channaveerappa M, Hoinkiss DC (2022) Towards free breathing 3D ASL imaging of the human liver using prospective motion correction. Magn Reson Med 88(2):711–726

70. Schalkx HJ, Petersen ET, Peters NHGM, Veldhuis WB, van Leeuwen MS, Pluim JPW, van den Bosch MAAJ, van Stralen M (2015) Arterial and portal venous liver perfusion using selective spin labelling MRI. Eur Radiol 25:1529–1540

71. Martirosian P, Pohmann R, Schraml C, Schwartz M, Kuestner T, Schwenzer NF, Scheffler K, Nikolaou K, Schick F (2019) Spatial-temporal perfusion patterns of the human liver assessed by pseudo-continuous arterial spin labeling MRI. Z Med Phys 29(2):173–183

72. Cox EF, Smith JK, Chowdhury AH, Lobo DN, Francis ST, Simpson J (2015) Temporal assessment of pancreatic blood flow and perfusion following secretin stimulation using noninvasive MRI. J Magn Reson Imaging 42(5):1233–1240

73. Taso M, Guidon A, Zhao L, Mortele KJ, Alsop DC (2019) Pancreatic perfusion and arterial-transit-time quantification using pseudocontinuous arterial spin labeling at 3T. Magn Reson Med 81(1):542–550

74. de Bazelaire CM, Duhamel GD, Rofsky NM, Alsop DC (2004) MR imaging relaxation times of abdominal and pelvic tissues measured in vivo at 3.0 T: preliminary results. Radiology 230(3):652–659

75. Schraml C, Schwenzer NF, Martirosian P, Claussen CD, Schick F (2008) Perfusion imaging of the pancreas using an arterial spin labeling technique. J Magn Reson Imaging 28(6):1459–1465

76. Erez O, Romero R, Jung E, Chaemsaithong P, Bosco M, Suksai M, Gallo DM, Gotsch F (2022) Preeclampsia and eclampsia: the conceptual evolution of a syndrome. Am J Obstet Gynecol 226(2S):S786–S803

77. Deloison B, Arthuis C, Benchimol G, Balvay D, Bussieres L, Millischer AE, Grévent D, Butor C, Chalouhi G, Mahallati H, Hélénon O, Tavitian B, Clement O, Ville Y, Siauve N, Salomon

LJ (2021) Human placental perfusion measured using dynamic contrast enhancement MRI. PLoS ONE 16(9):e0256769

78. Shao X, Liu D, Martin T, Chanlaw T, Devaskar SU, Janzen C, Murphy AM, Margolis D, Sung K, Wang DJJ (2018) Measuring human placental blood flow with multidelay 3D GRASE pseudocontinuous arterial spin labeling at 3T. J Magn Reson Imaging 47(6):1667–1676

79. Herrera CL, Wang Y, Udayakumar D, Xi Y, Do QN, Lewis MA, Owen DM, Fei B, Spong CY, Twickler DM, Madhuranthakam AJ (2023) Longitudinal assessment of placental perfusion in normal and hypertensive pregnancies using pseudo-continuous arterial spin-labeled MRI: preliminary experience. Eur Radiol 33(12):9223–9232

80. Zun Z, Zaharchuk G, Andescavage NN, Donofrio MT, Limperopoulos C (2017) Non-invasive placental perfusion imaging in pregnancies complicated by fetal heart disease using velocity-selective arterial spin labeled MRI. Sci Rep 7(1):16126

81. Guttmacher AE, Maddox YT, Spong CY (2014) The human placenta project: placental structure, development, and function in real time. Placenta 35(5):303–304

82. Liu D, Shao X, Danyalov A, Chanlaw T, Masamed R, Wang DJJ, Janzen C, Devaskar SU, Sung K (2020) Human placenta blood flow during early gestation with pseudocontinuous arterial spin labeling MRI. J Magn Reson Imaging 51(4):1247–1257

83. Zun Z, Limperopoulos C (2018) Placental perfusion imaging using velocity-selective arterial spin labeling. Magn Reson Med 80(3):1036–1047

84. Aramendia-Vidaurreta V, Echeverria-Chasco R, Vidorreta M, Bastarrika G, Fernandez-Seara MA (2021) Quantification of myocardial perfusion with vasodilation using arterial spin labeling at 1.5 T. J Magn Reson Imaging 53(3):777–788

85. Aramendia-Vidaurreta V, Solis-Barquero SM, Ezponda A, Vidorreta M, Echeverria-Chasco R, Pascual M, Bastarrika G, Fernandez-Seara MA (2023) Assessment of splenic switch-off with arterial spin labeling in adenosine perfusion cardiac MRI. J Magn Reson Imaging 58(1):147–156

86. Li X, Metzger GJ (2013) Feasibility of measuring prostate perfusion with arterial spin labeling. NMR Biomed 26(1):51–57

87. Pretorius ES, Roberts DA (2004) Continuous arterial spin-labeling perfusion magnetic resonance imaging of the human testis. Acad Radiol 11(1):106–110

88. Zhang Z, Karasan E, Gopalan K, Liu C, Lustig M (2021) DiSpect: displacement spectrum imaging of flow and tissue perfusion using spin-labeling and stimulated echoes. Magn Reson Med 86(5):2468–2481

89. Zhou L, Zhang Q, Spincemaille P, Nguyen TD, Morgan J, Dai W, Li Y, Gupta A, Prince MR, Wang Y (2021) Quantitative transport mapping (QTM) of the kidney with an approximate microvascular network. Magn Reson Med 85(4):2247–2262

90. Shao X, Ma SJ, Casey M, D'Orazio L, Ringman JM, Wang DJJ (2019) Mapping water exchange across the blood–brain barrier using 3D diffusion-prepared arterial spin labeled perfusion MRI. Magn Reson Med 81(5):3065–3079

91. Fan H, Bunker L, Wang Z, Durfee AZ, Lin D, Yedavalli V, Ge Y, Zhou XJ, Hillis AE, Lu H (2024) Simultaneous perfusion, diffusion, T2*, and T1 mapping with MR fingerprinting. Magn Reson Med 91(2):558–569

92. Hales PW, Clark CA (2013) Combined arterial spin labeling and diffusion-weighted imaging for noninvasive estimation of capillary volume fraction and permeability-surface product in the human brain. J Cereb Blood Flow Metab 33(1):67–75

93. Wang J, Fernández-Seara MA, Wang S, St Lawrence KS (2007) When perfusion meets diffusion: in vivo measurement of water permeability in human brain. J Cereb Blood Flow Metab 27(4):839–849

94. Ahn H-S, Jung Y, Park S-H (2022) Measuring glomerular blood transfer rate in kidney using diffusion-weighted arterial spin labeling. Magn Reson Med 88(6):2408–2418